Annals of Biomedical Engineering, Vol. 43, No. 12, December 2015 *(© 2015)* pp. 3015–3024
DOI: 10.1007/s10439-015-1360-1

Analysis of the Effects of Normal Walking on Ankle Joint Contact Characteristics After Acute Inversion Ankle Sprain

JI YONG BAE,[1] KYUNG SOON PARK,[2] JONG KEUN SEON,[2] and INSU JEON[3]

[1]Center for Analytical Instrumentation Development, Korea Basic Science Institute, 169-148 Gwahak-ro, Yuseong-gu, Daejeon 305-806, Republic of Korea; [2]The Center for Joint Disease, Hwasun Hospital, Chonnam National University, 160 Ilsimri, Hwasun-Eup, Hwasun-Gun, Jeonnam 519-809, Republic of Korea; and [3]School of Mechanical Engineering, Chonnam National University, 300 Yongbong-dong, Buk-gu, Gwangju 500-757, Republic of Korea

(Received 4 December 2014; accepted 9 June 2015; published online 16 June 2015)

Associate Editor Joel D. Stitzel oversaw the review of this article.

Abstract—To show the causal relationship between normal walking after various lateral ankle ligament (LAL) injuries caused by acute inversion ankle sprains and alterations in ankle joint contact characteristics, finite element simulations of normal walking were carried out using an intact ankle joint model and LAL injury models. A walking experiment using a volunteer with a normal ankle joint was performed to obtain the boundary conditions for the simulations and to support the appropriateness of the simulation results. Contact pressure and strain on the talus articular cartilage and anteroposterior and mediolateral translations of the talus were calculated. Ankles with ruptured anterior talofibular ligaments (ATFLs) had a higher likelihood of experiencing increased ankle joint contact pressures, strains and translations than ATFL-deficient ankles. In particular, ankles with ruptured ATFL + calcaneofibular ligaments and all ruptured ankles had a similar likelihood as the ATFL-ruptured ankles. The push off stance phase was the most likely situation for increased ankle joint contact pressures, strains and translations in LAL-injured ankles.

Keywords—Finite element simulation, Walking experiment, Lateral ankle ligament injury, Contact pressure, Contact strain, Anteroposterior translation, Mediolateral translation.

INTRODUCTION

Acute ankle sprain is a common sports injury in which the ligaments of the ankle are torn, partially or completely, due to sudden and abnormal stretching. It is caused by an excessive inversion or eversion of the ankle joint.[5,19] Up to 80% of sprains are associated with an inversion mechanism.[13,23] As a result, the lateral ankle ligaments (LALs) are those most frequently injured by inversion ankle sprain. A common LAL injury is injury of the anterior talofibular ligament (ATFL), which is often accompanied by injury of the calcaneofibular ligament (CFL) or both the CFL and posterior talofibular ligament (PTFL).[11,12,22] Nonoperative treatments are primarily applied for these LAL injuries.[2,26] However, when adequate nonoperative treatment fails, LAL injuries may result in lateral ankle instability (LAI), which alters the kinematics of the tibiotalar joint[8,15,17,30] and leads to an increase of *in vivo* cartilage contact strains and deformation.[6,34] It has been reported that 10–40% of lateral ankle sprain patients may experience chronic LAI.[16,20,33]

Chronic LAI leads to cartilage degeneration and the development of ankle joint osteoarthritis.[7,15,17,18,21,24,29,31,32] Long-term follow-up studies have reported that osteoarthritis develops in 13–78% of patients with LAI beyond 10 years.[7,15,21] Moreover, recent patient studies have reported that LAL lesions are the main cause of ligamentous posttraumatic ankle arthritis.[17,31,32] Although the aforementioned studies have reported a relationship between LAI and osteoarthritis, the effects of LAL injury types—LAL deficiencies and ruptures—on *in vivo* ankle joint kinematics have not yet been clearly described.

Recently, the ankle joint structure at the midstance phase of walking has been studied using dual-orthogonal fluoroscopy and a 3D ankle joint model, which was reconstructed using magnetic resonance (MR) images, to understand the ankle joint function and etiology of osteoarthritis.[6,8,34] The effects of ATFL-deficient LAI on the motion of the tibiotalar joint has been quantified for weight-bearing loading conditions by Caputo *et al.*[8] Wan *et al.*[34] determined *in vivo*

Address correspondence to Insu Jeon, School of Mechanical Engineering, Chonnam National University, 300 Yongbong-dong, Buk-gu, Gwangju 500-757, Republic of Korea. Electronic mail: i_jeon@chonnam.ac.kr

0090-6964/15/1200-3015/0 © 2015 Biomedical Engineering Society

cartilage thickness and articular cartilage contact strain distributions in normal ankle joints under full body weight loading conditions. Bischof *et al.*[6] investigated *in vivo* cartilage contact strain and its peak value translations in both ATFL-deficient and normal ankle joints. Although these studies provided valuable data on *in vivo* ankle joint cartilage contact conditions with an intact or deficient ATFL under weight-bearing conditions, they did not show the effects of normal walking with an injured LAL ankle joint on the *in vivo* cartilage contact situation.

Here, we have constructed a complex 3D finite element (FE) model of a foot with an intact ankle joint. Using the intact ankle model, two different ATFL-deficient models and three LAL-ruptured models (ATFL, ATFL + CFL, and ATFL + CFL + PTFL ruptures) were fabricated for various LAL injury types. FE simulations were carried out using these models to evaluate ankle cartilage contact pressures and strains as well as *in silico* tibiotalar joint motions under normal walking conditions. The four stance phases of the gait cycle—heel strike, foot flat, mid-stance, and push off—were simulated. In addition, barefoot walking experiments were carried out to provide the boundary conditions for the FE simulations and to validate the simulation results. The purpose of this study was to show the causal relationship between normal walking on injured LAL ankle joints resulting from acute inversion ankle sprain and ankle joint contact characteristics.

MATERIALS AND METHODS

3D Reconstruction and Geometric Modeling

The study protocol was approved by the Institutional Review Board of our institution (RTOS1033). T1 MR images of the left foot at the neutral foot position were taken from a volunteer (33-year-old male, 70 kg, 686 N) with no history of ankle joint injuries or pathologies. The height of MR scan region from the sole of the foot was 168 mm. The MR scan was performed using a 3T-MR scanner (Signa Excite 3.0T; GE HealthCare, USA), which was equipped with a standard quadrature knee coil. The scan parameters selected were as follows: echo time/repetition time (1.46 ms/5.84 ms), slice thickness (2.8 mm), gap between two reconstructed MR image (0.7 mm), total number of MR images (240), field of view (290×290 mm^2), acquisition matrix (512×256; reconstructed to 512×512), pixel bandwith (244 kHz), acquisition time (8 min 59 s), and optimal pixel size (0.566 mm). In order to maintain the non-weight-bearing condition of the ankle joint, the volunteer maintained a supine position for at least 30 min before the scan. Using MR images, 28 bony structures, including tibia, fibula, talus, calcaneus, cuboid, navicular, cuneiforms, metatarsals, components of the phalanges, articular cartilages, and encapsulated soft tissue were reconstructed three-dimensionally using the commercial software MIMICS (v10.1; Materialise, Belgium). Using each reconstructed model, the geometric solid model of the foot was fabricated using the software Rapidform 2006 (Inus Technology Inc., Korea).

FE Modeling and Material Properties

On the geometric model, the 3D FE model of the intact foot was constructed using the commercial software PATRAN (v2008; MSC Software Corporation, USA) (Figs. 1a and 1b). The tetrahedral solid element was used for all bony structures and their articular cartilages. The tetrahedral hybrid continuum element, which can be suitably used for hyperelastic materials, was used for the encapsulated soft tissues. The seven major ankle ligaments (ATFL/PTFL, CFL, anterior/posterior tibiotalar ligament, tibionavicular ligament, and tibiocalcaneal ligament), plantar fascia, and foot ligaments were attached as 1D truss elements at the anatomically corresponding insertion sites of the bony FE models. These ligaments and plantar fascia were considered to have a physiological cross-sectional area (PCSA)[10,28,36] and a response to tension only according to their physiological behaviors. Six muscle groups, including the triceps surae/Achilles tendon, flexor hallucis longus, flexor digitorum longus, tibialis posterior, peroneus brevis, and peroneus longus, were attached as axial connector elements at the anatomically appropriate sites in the FE models. These muscle groups, which constitute the major plantar flexors of the foot, control the movement and balance of the foot with their muscle contractile forces. The insertion sites of all ligaments and muscles were determined using MR images. We checked 240 MR images of the ankle joint to select the sites. We discussed the anatomic suitability of the sites with orthopedic surgeons. The process of discussions and modifications for the selected insertion sites were repeated until the suitability of those sites was confirmed by surgeons. As a result, we determined the accurate insertion sites of the ligaments and muscles on the 3D reconstructed model and transferred the sites on the 3D FE model.

The bony structures, articular cartilages, plantar fascia, and ligaments were assumed to be homogeneous, isotropic, and linear elastic material.[1,14,36] The encapsulated soft tissue was considered to be incompressible, isotropic, and nonlinear hyperelastic material, which can be modeled using the first-order Ogden model. For its governing equation, hyperelastic strain energy potential U was defined as

$$U = \frac{2\mu}{\alpha^2}(\lambda_1^\alpha + \lambda_2^\alpha + \lambda_3^\alpha - 3), \quad (1)$$

where α is a material constant, μ is the initial shear modulus, and λ_i ($i = 1, 2, 3$) is the deviatoric principal stretch along the ith orthogonal and principal direction. For the FE simulation, values of $\alpha = 5.5$ and $\mu = 0.0375$ MPa were selected.[9]

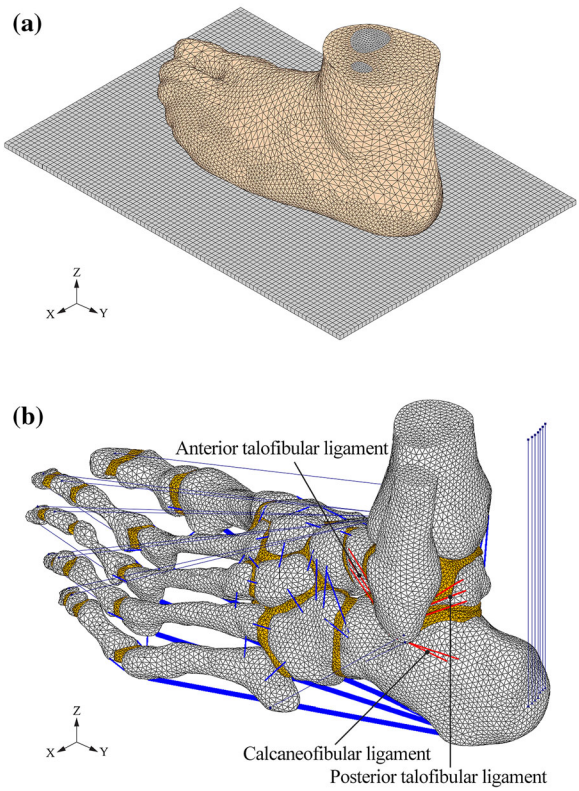

FIGURE 1. 3D FE model of the human foot (a) with and (b) without the encapsulated soft tissue.

To represent the ankle joint with a series of LAL injuries, three LAL rupture models (ATFL, ATFL + CFL, and ATFL + CFL + PTFL rupture models) and two ATFL-deficient models were created. The LAL rupture models were made by removing the ATFL, CFL, and PTFL, respectively, in the intact foot model. The ATFL-deficient models were made by lowering the elastic modulus compared with that of the intact ATFL. All material properties used for the FE simulation are shown in Table 1.[1,9,10,14,28,36] The entire FE model was generated at the unloaded neutral position. Fine FE meshes of 416,340 elements and 101,000 nodes were used, and very fine meshes were adopted around the plantar soft tissue. Therefore, the calculated results are insensitive to further refinements or increases in the number of elements.[3,4]

Walking Experiments

To obtain the boundary condition for the FE simulation of normal walking and to validate the simulation results, the volunteer who participated in the MR scan performed walking experiments using a force platform system (EMED-c50; Novel, Germany) and high-resolution video equipment (NX20; Samsung, Korea). Experimental data were recorded at a sampling rate of 25 Hz for the force platform system and 30 Hz for the video equipment.

During the walking experiment, the vertical ground reaction force (GRF), tibial inclination relative to the ground, plantar pressure distributions, and plantar

TABLE 1. Material properties of each tissue.

Tissue	Elastic modulus (MPa)		Poisson's ratio
Bony structures	7300.0		0.3
Cartilages	10.0		0.4
Ground	72,000.0		0.3
	Elastic modulus (MPa)	Poisson's ratio	PCSA (mm^2)
Plantar fascia	350.0	0.4	290.7
ATFL	255.5	0.4	12.9
PTFL	216.5	0.4	21.9
CFL	512.0	0.4	9.7
ATTL	184.5	0.4	13.5
PTTL	99.5	0.4	22.6
TCL	512.0	0.4	9.7
TNL	320.7	0.4	7.1
Other ligaments	260.0	0.4	18.4
ATFL-deficient #1	180	0.4	290.7
ATFL-deficient #2	120	0.4	290.7
Encapsulated soft tissue	1st-order Ogden hyperelastic model for incompressive materials $\alpha = 5.5$, $\mu = 0.0375$ MPa		

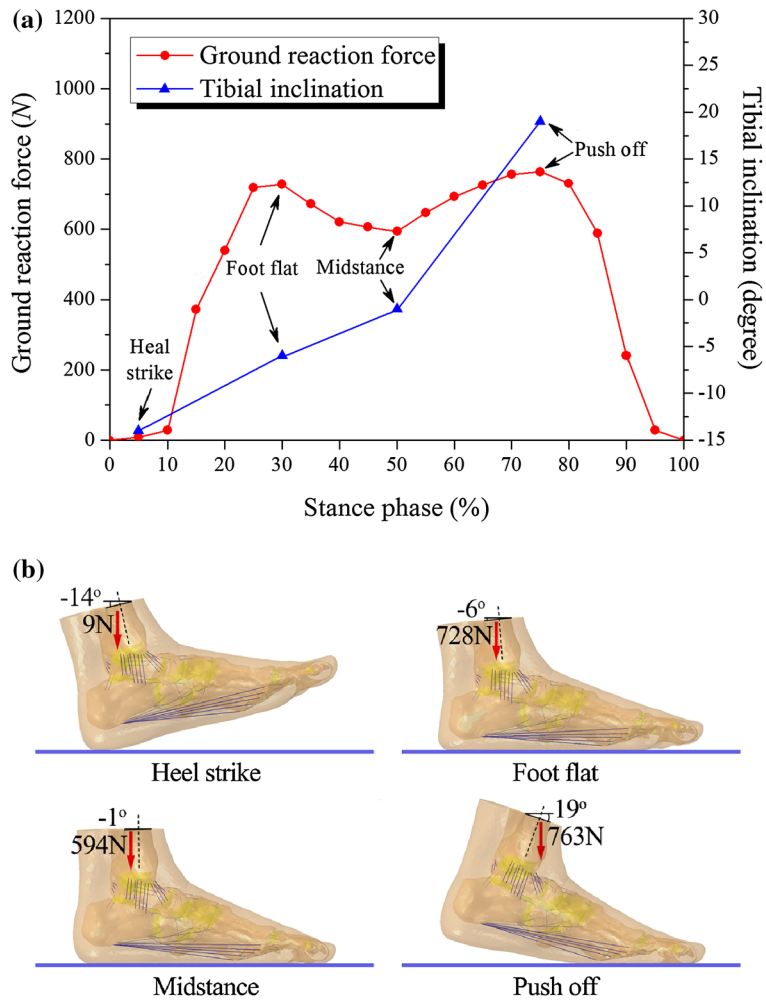

FIGURE 2. Vertical ground reaction forces and foot positions at the four stance phases.

contact area were obtained following the stance phases (Fig. 2a). The measured vertical GRFs and tibial inclinations were used as the boundary conditions for the walking simulation (Fig. 2b). The plantar pressure values and distributions and plantar contact area for each stance phase were compared with the results of the FE simulation (Fig. 3).

Walking Simulation

For the barefoot walking simulation, the 3D FE foot model was initially aligned parallel to the ground and rotated −14° by displacement controls, which is the tibial inclination relative to the ground, and a vertical GRF of 9 N was applied to establish the heel strike position (Fig. 2b). Then, the three stance phases—foot flat, midstance, and push off—were simulated as subsequent steps by applying prescribed vertical GRFs (728 N, 594 N, and 763 N) and tibial inclinations (−6°, −1°, and 19°), respectively (Fig. 2b). The vertical GRFs of each phase were applied to the superior surfaces of the tibia and fibula, and the ground was fixed along all directions throughout the stance phases to prevent translation and rotation. To apply the tibial inclination angles of each phase to the foot model, the superior surfaces of the tibia, fibula, and encapsulated soft tissue were rotated together around the reference point. During the walking simulation, other GRF and tibial inclination components in the transverse and coronal planes were ignored in order to decrease the complexity of the simulation.

To simulate actual walking performance, the muscle contractile forces of each stance phase were applied to the modeled axial connector elements. Generally, the muscle forces during barefoot walking were calculated based on normalized electromyography (EMG) data and PCSA values.[25,27,35] For all muscles in this study, we adopted the muscle forces calculated by the linear relationship between EMG amplitude and muscle tension.[27]

Frictionless contact between the articular cartilage surfaces of the tibia, fibula, talus, and calcaneus was

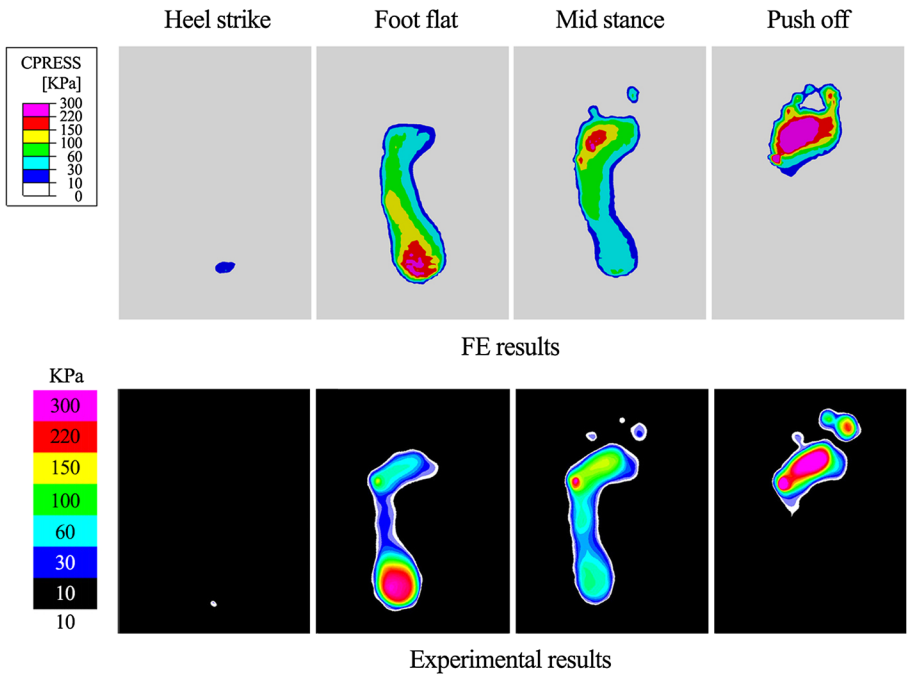

FIGURE 3. Plantar pressure distributions obtained from FE analysis and experimental measurements during walking: heel strike, foot flat, midstance, and push off.

TABLE 2. Applied load, muscle forces, and boundary conditions used for walking simulation.

	Heel strike	Foot flat	Midstance	Push off
Tibial inclination angles (°)	14	−6	−1	19
Vertical ground reaction force (N)	9	728	594	763
Triceps surae/Achilles tendon (N)	–	375	950	1600
Flexor hallucis longus (N)	–	10	30	160
Flexor digitorum longus (N)	–	11	48	88
Tibialis anterior (N)	–	0	80	–
Tibialis posterior (N)	–	85	56	127
Peroneus brevis (N)	–	2.5	25	50
Peroneus longus (N)	–	2.5	25	50

defined.[9] A friction coefficient of 0.6 was used between the ground and plantar surface.[37] All loads, including muscle forces and boundary conditions, used in this study for each stance phase are shown in Table 2. The FE simulation of each model was carried out using the commercial software ABAQUS (v6.8.1; Dassult Systemes, France).

RESULTS

Figure 3 shows the barefoot plantar pressure distributions obtained from the FE simulation and the experimental measurements during walking. The concentrated plantar contact pressure occurred in the center of the heel region at the heel strike and foot flat phases, and the region gradually moved to the forefoot at the midstance and push off phases. The experimental results showed a translation of the concentrated plantar pressure regions similar to that of the simulation results. The peak plantar pressures obtained from the simulation at the heel strike, foot flat, midstance, and push off phases were 0.03, 0.31, 0.32, and 0.65 MPa, respectively, which were 33, 3, 12, and 6% higher, respectively, than those of the experiment (0.02, 0.30, 0.28, and 0.61 MPa, respectively). In terms of the plantar contact area, the simulations provided 3.13, 86.07, 90.01, and 54.49 cm^2, respectively, at the stance phase, which showed differences of 20, 5, 1, and 6%, respectively, from the experimental results (2.51, 81.53, 91.02, and 51.11 cm^2, respectively). Although the differences in values between the simulation and experimental results at the heel strike phase were relatively larger than the differences in the other phases, the

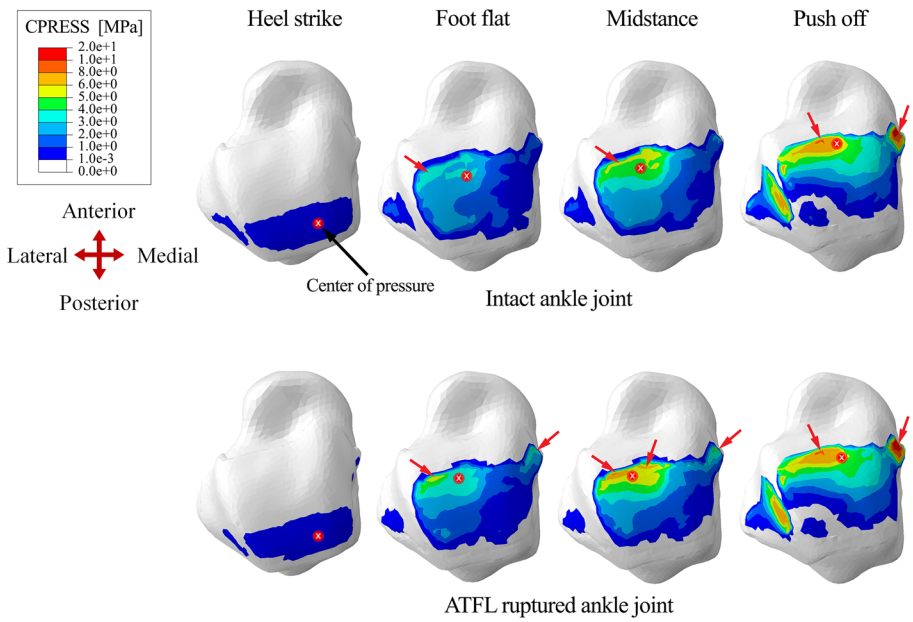

FIGURE 4. Contact pressure distributions and centers of pressure on the talus articular cartilage for the intact and ATFL-ruptured ankle joints during walking: heel strike, foot flat, midstance, and push off.

magnitude of the values was very small. Therefore, the FE simulation results showed good agreement with the experimental results. Based on these results, we were able to confirm the suitability of the FE simulation technique in this study.

Contact Pressure Distributions

Figure 4 shows the calculated contact pressure distributions and centers of pressure on the articular cartilage of the talus during normal walking using the intact and ATFL-ruptured ankle joint models. With the progression of the walking phases, the contact pressures on the cartilage gradually increased and the contact regions expanded in both models. The concentrated contact pressure regions moved from the lateral to the medial side and from the posterior to the anterior side in both models (Fig. 4). In the ATFL-ruptured ankle joint model, the concentrated contact pressures increased at each stance phase, and the concentrated pressure regions were more medially translated at the foot flat and midstance phases compared with those of the intact model (see the arrows in Fig. 4). At the push off stance phase, similar concentrated pressure regions were found in both models.

Peak Contact Pressures

Figure 5a shows the calculated peak contact pressures on the talus cartilage using the intact and injured LAL ankle joint models at the four stance phases (heel

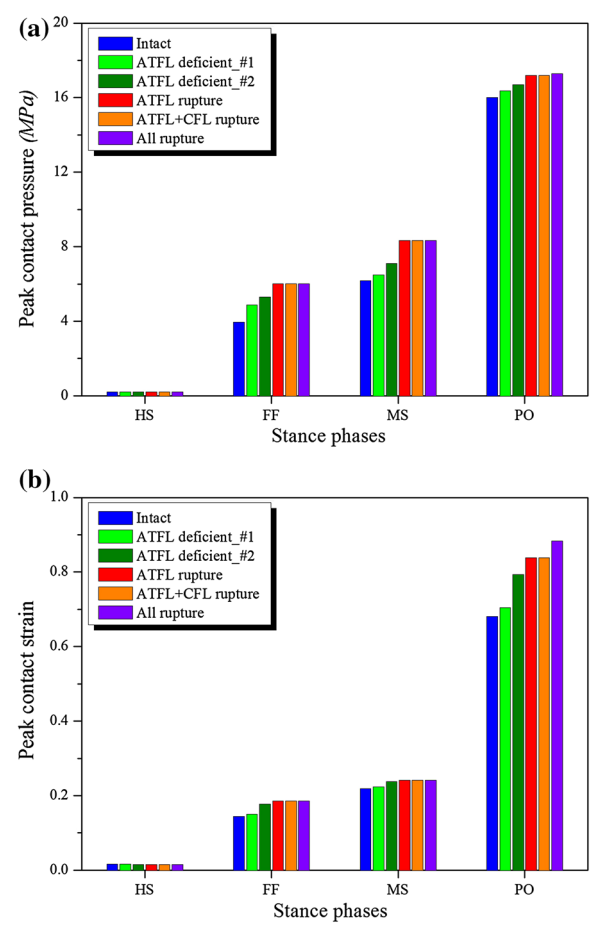

FIGURE 5. (a) Calculated peak contact pressures and (b) peak strains across the ankle joint during walking.

strike, foot flat, midstance, and push off). While the peak contact pressures at the heel strike stance phase in all models were very small and similar to each other at 0.21–0.22 MPa, with the progression of the stance phase, significant increases in the values were detected in all models. In particular, a rapid increase of the values was observed at the push off stance phase. In the intact model, the peak contact pressures at the foot flat, midstance, and push off stance phases were 3.95, 6.18, and 16.02 MPa, respectively. In the two ATFL-deficient models, these peak values increased gradually (4.87, 6.54, and 16.37 MPa, respectively, in the ATFL-deficient #1 model and 5.37, 7.12, and 16.79 MPa, respectively, in the ATFL-deficient #2 model). The values of the ATFL-ruptured model were 6.01, 8.33, and 17.24 MPa, respectively, which were higher than those of the intact and two ATFL-deficient models. In the ATFL + CFL ruptured and all ruptured models, the values obtained were nearly the same as those of the ATFL ruptured model at each stance phase.

Peak Contact Strains

Figure 5b shows the calculated peak contact strains of the six models, all of which increased following each stance phase. Similar to the peak contact pressures, a rapid increase in the values was observed at the push off stance phase. There were no significant differences in peak contact strain among the models at the heel strike stance phase, which was around 0.015–0.017. In the intact model, those values were 0.144, 0.219, and 0.681, respectively, at the foot flat, midstance, and push off phases. The ATFL-deficient #1 (0.150, 0.224, and 0.705), ATFL-deficient #2 (0.178, 0.238, and 0.793), and ATFL-ruptured (0.186, 0.241, and 0.838) models showed an increase in those values compared with those of the intact model. The contact peak strains of the ATFL + CFL-ruptured model were the same as those of the ATFL-ruptured model. In the all ruptured model, the values obtained were almost the same as those of the ATFL-ruptured model at the foot flat and midstance phases. However, at the push off phase, the value was slightly increased to 0.883 (5% increase).

Anteroposterior Translation

Figure 6a shows the anteroposterior translation of the talus in the intact ankle model and the differences in translation between the intact model and the other models at the foot flat, midstance, and push off phases, respectively. In the intact ankle model, the talus was translated anteriorly, and the translation increased as the walking phases progressed (3.67, 5.79, and 14.42 mm, respectively). At each stance phase, positive differences in the anterior translation were observed in the ATFL-deficient #1 (0.05, 0.05, and 0.12, respectively), ATFL-deficient #2 (0.19, 0.17, and 0.25, respectively), and ATFL-ruptured (0.26, 0.25 and 0.35, respectively) models. The differences at all phases in the ATFL + CFL-ruptured and all ruptured models were almost the same as those of the ATFL-ruptured model.

Based on the sum of the differences and the intact model translations at each stance phase, a more anteriorly translated talus was found in the LAL injury models. The ATFL-ruptured model showed a larger translation than the ATFL-deficient #1 and #2 models at each stance phase. The ATFL-deficient #1 model showed a smaller translation than the ATFL-deficient #2 model. The translations of the ATFL + CFL-ruptured and all ruptured ankle models were almost the same as those of the ATFL-ruptured model.

Mediolateral Translation

The mediolateral translation of the talus in the intact ankle model and the translation differences between the intact model and the other models at each stance phase are shown in Fig. 6b. In the intact ankle model, the talus was medially translated at the foot flat phase (0.07 mm), and the translation increased at the midstance phase (0.14 mm). At the push off phase, contralateral translation was observed (lateral translation of 0.1 mm). The positive medial differences at each stance phase (in the ATFL-deficient #1 model, 0.008, 0.007, and 0.003, respectively; in the ATFL-deficient #2 model, 0.034, 0.026, and 0.011, respectively; and in the ATFL-ruptured model, 0.041, 0.038, and 0.015, respectively) show a more medially translated talus in the injured LAL models than in the intact model. In addition, at the push off phase, contralateral translations from the injured LAL models were observed. However, all the mediolateral translations and their differences at each stance phase were very small compared with those of the anteroposterior translation of the talus.

DISCUSSION

As the walking phases progressed, the contact pressure and strain on the talus articular cartilage increased gradually, and the regions of concentrated contact pressure on the cartilage were anteromedially translated. The anteroposterior translation of the talus increased following the walking phases. In particular, the contact pressures and strains and the anteroposterior translation increased rapidly at the push off phase. The mediolateral translation increased until the

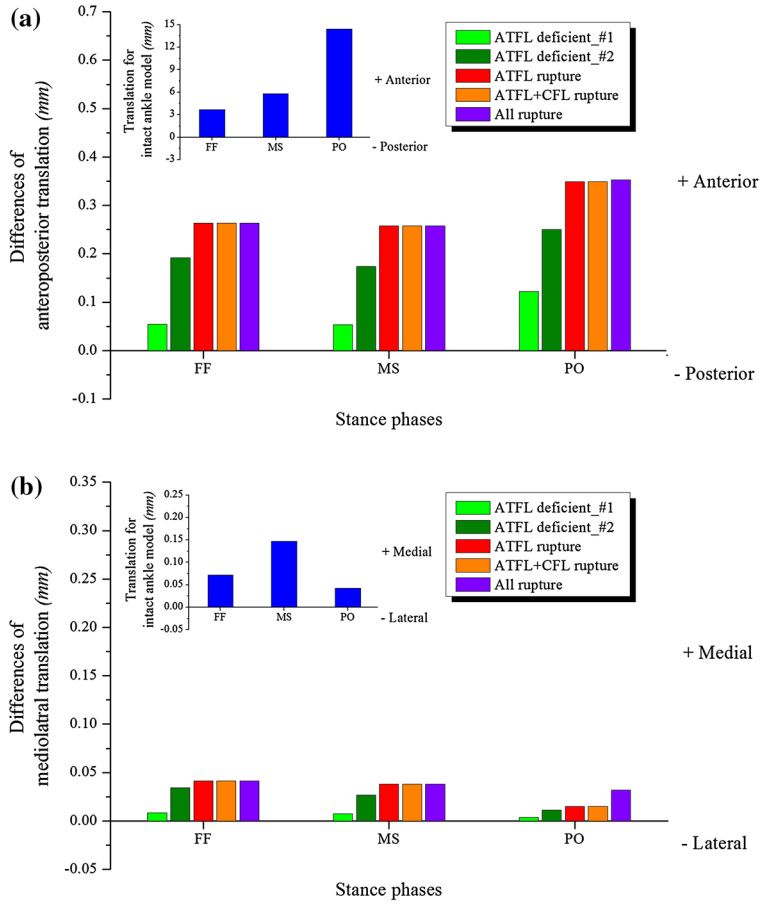

FIGURE 6. (a) Calculated anteroposterior and (b) mediolateral translation of the talus and their translation differences between the intact model and the other models during walking.

midstance phase was reached and decreased at the push off phase. However, the magnitudes of the mediolateral translations were very small compared with the anteroposterior translation.

As the mechanical property of the ATFL decreased (ATFL-deficient state), the peak contact stress and strain and the translations increased at each stance phase. Those values were the highest in the ATFL-ruptured model. In the ATFL + CFL-ruptured and all ruptured ankle joint models, all contact parameters and translations were almost the same as those of the ATFL-ruptured model. Therefore, it was found that the ATFL contributed significantly to the LAI of the ankle joint during normal walking. However, the CFL and PTFL provided relatively small contributions compared with the ATFL.

The contact strain distribution in the tibiotalar joint at the midstance phase was experimentally measured by Bischof *et al.*,[6] who showed that the peak contact strain at 100% body weight was 29 ± 8% on the injured ATFL ankle joint and 21 ± 5% on the intact joint. In this study, we obtained values of 22.4 and 23.8% in the AFTL-deficient #1 and #2 models, respectively, and 21.9% in the intact joint model at the midstance phase. This finding shows that our calculated strain values are well confined within the measured results. Bischof *et al.*[6] also reported that the peak contact strain region on the injured ankle significantly translated anteriorly and medially. Our results showed that the peak contact pressure regions were anteromedially translated (Fig. 4). Because we assumed cartilage to be a linear elastic material, the translation of the peak contact pressure should be in accordance with that of the peak contact strain. Therefore, translation of the peak contact parameter in this study coincided well with the results of Bischof *et al.*[6]

In the intact ankle model, contact pressure in the medial side of the talus cartilage increased gradually during walking (Fig. 4). These results might be explained by the fact that the talus rotated internally and increased the contact force between the medial portion of the talus articular cartilage and the tibia cartilage. The same phenomenon was found in the ankle joint with ATFL rupture; however, the peak

contact pressure values were higher than those of the intact model (Fig. 4). This result was due to the altered kinematics of the ankle joint as a result of the loss of mechanical function of the ATFL, and it might be evidence of the role of the ATFL in the ankle joint in resisting abnormal internal rotation of the talus. These results were consistent with the findings in the literature that the ATFL provides resistance to the internal rotation of the talus.[8,29] In addition, our results were able to support the hypothesis that LAI induced cartilage damage in the medial portion of the talus as a result of abnormal kinematics[8,15,17,30] and that the increased internal rotation of the talus caused by ATFL injury changed the contact mechanism due to the articular surface shape of the medial malleolus.[6,8]

Caputo *et al.*[8] reported that significant increases of the anterior translation were measured in the ATFL injury ankle compared with the intact ankle. In contrast, insignificant differences in the medial translation were found between the intact and the ATFL injury ankles. Our results also showed significant anterior translation but very little medial translation of the talus in the injured LAL ankle models compared with the intact ankle model.

In this study, we saw that a deficient ATFL and LAL rupture could cause increased contact pressures and strains during normal walking. The ATFL rupture ankles showed greater values of the contact parameters than the ATFL-deficient ankles. The ATFL + CFL-ruptured and all ruptured ankles showed similar contact parameter values as those of the ATFL-ruptured ankles. Moreover, the push off phase placed the most severe burden on the injured LAL ankle joints, which could be a significant driving force behind increasing the contact pressures and strains. Therefore, these altered and increased contact pressures and strains caused by LAL injuries could contribute to cartilage degeneration and the development of ankle osteoarthritis.[4,32]

This study has some limitations. First, a single ankle joint was used for the simulations. To see a more general trend of changes in contact pressures and strains and translations in the tibiotalar joint, statistical analyses using simulations of various ankle joint models are necessary. Second, the elastic moduli of the deficient ATFL were not measured. We selected them by lowering the modulus of the intact ATFL in order to simplify our problem. Finally, we assumed that the cartilages and ligaments exhibited elastic material behaviors in our simulations. Because we performed an FE simulation of four stance phases of a gait cycle, which took the volunteer only 0.8 s, the assumption of linear elastic material behavior could be acceptable for our simulations. However, to obtain more accurate values of the contact parameters and translations of the tibiotalar joint during gait cycles, simulations of more gait cycles using the time-dependent material properties of cartilages and ligaments are necessary.

In summary, our computer model of an individual with an injured LAL representing a significant inversion ankle sprain showed altered ankle joint kinematics during normal walking. The injured LAL increased contact pressure and strain on the talus articular cartilage and translation of the talus. Therefore, normal walking on an injured LAL could be a significant cause of the alteration of contact characteristics. The ATFL-ruptured ankles showed a higher likelihood of experiencing increased ankle joint contact pressure, strain and translations than ATFL-deficient ankles. The ATFL + CFL-ruptured and all ruptured ankles showed a similar likelihood as the ATFL ruptured ankles. This study showed that in injured LAL ankles, the push off phase is the most likely stance for increasing ankle joint contact pressures and strains.

ACKNOWLEDGEMENT

This work was supported by the National Research Foundation of Korea (NRF) Grant funded by the Korea government (MEST) (No. 2012R1A2A2A0104 6128).

CONFLICT OF INTEREST

No conflicts of interest present in this study.

REFERENCES

[1]Anderson, D. D., J. K. Goldsworthy, K. Shivanna, N. M. Grosland, D. R. Pedersen, T. P. Thomas, Y. Tochigi, J. L. Marsh, and T. D. Brown. Intra-articular contact stress distributions at the ankle throughout stance phase-patient-specific finite element analysis as a metric of degeneration propensity. *Biomech. Model Mechanobiol.* 5(2–3):82–89, 2006.

[2]Ardevol, J., I. Bolibar, V. Belda, and S. Argilaga. Treatment of complete rupture of the lateral ligaments of the ankle: a randomized clinical trial comparing cast immobilization with functional treatment. *Knee Surg. Sports Traumatol. Arthrosc.* 10(6):371–377, 2002.

[3]Bae, J. Y., D. S. Kwak, K. S. Park, and I. Jeon. Finite element analysis of the multiple drilling technique for early osteonecrosis of the femoral head. *Ann. Biomed. Eng.* 41(12):2528–2537, 2013.

[4]Bae, J. Y., K. S. Park, J. K. Seon, D. S. Kwak, I. Jeon, and E. K. Song. Biomechanical analysis of the effects of medial meniscectomy on degenerative osteoarthritis. *Med. Biol. Eng. Comput.* 50(1):53–60, 2012.

[5]Balduini, F. C., and J. Tetzlaff. Historical perspectives on injuries of ligaments of the ankle. *Clin. Sports Med.* 1:3–12, 1982.

[6]Bischof, J. E., C. E. Spritzer, A. M. Caputo, M. E. Easley, J. K. DeOrio, J. A. Nunley, II, and L. E. DeFrate. In vivo cartilage contact strains in patients with lateral ankle instability. *J. Biomech.* 43(13):2561–2666, 2010.
[7]Canale, S. T., and R. H. Belding. Osteochondral lesions of the talus. *J. Bone Joint Surg. Am.* 62(1):97–102, 1980.
[8]Caputo, A. M., J. Y. Lee, C. E. Spritzer, M. E. Easley, J. K. DeOrio, J. A. Nunley, II, and L. E. DeFrate. In vivo kinematics of the tibiotalar joint after lateral ankle instability. *Am. J. Sports Med.* 37(11):2241–2248, 2009.
[9]Chen, W. M., V. Phyau-Wui Shim, S. B. Park, and T. Lee. An instrumented tissue tester for measuring soft tissue property under the metatarsal heads in relation to metatarsophalangeal joint angle. *J. Biomech.* 44(9):1801–1804, 2011.
[10]Corazza, F., J. J. O'Connor, A. Leardini, and V. Parenti. Castelli. Ligament fibre recruitment and forces for the anterior drawer test at the human ankle joint. *J. Biomech.* 36(3):363–372, 2003.
[11]DiGiovanni, B. F., G. Partal, and J. F. Baumhauer. Acute ankle injury and chronic lateral instability in the athlete. *Clin. Sports Med.* 23(1):1–19, 2004.
[12]Ferran, N. A., and N. Maffulli. Epidemiology of sprains of the lateral ankle ligament complex. *Foot Ankle Clin.* 11(3):659–662, 2006.
[13]Fong, D. T., Y. Y. Chan, K. M. Mok, P. Yung, and K. M. Chan. Understanding acute ankle ligamentous sprain injury in sports. *Sports Med. Arthrosc. Rehabil. Ther. Technol.* 1:14, 2009.
[14]Gefen, A., M. Megido-Ravid, Y. Itzchak, and M. Arcan. Biomechanical analysis of the three-dimensional foot structure during gait: a basic tool for clinical applications. *J. Biomech. Eng.* 122:630–639, 2000.
[15]Harrington, K. D. Degenerative arthritis of the ankle secondary to long-standing lateral ligament instability. *J. Bone Joint Surg. Am.* 61(3):354–361, 1979.
[16]Hintermann, B., V. Valderrabano, A. Boss, H. H. Trouillier, and W. Dick. Medial ankle instability: an exploratory, prospective study of fifty-two cases. *Am. J. Sports Med.* 32(1):183–190, 2004.
[17]Hintermann, B., A. Boss, and D. Schafer. Arthroscopic findings in patients with chronic ankle instability. *Am. J. Sports Med.* 30(3):402–409, 2002.
[18]Hirose, K., G. Murakami, T. Minowa, H. Kura, and T. Yamashita. Lateral ligament injury of the ankle and associated articular cartilage degeneration in the talocrural joint: anatomic study using elderly cadavers. *J. Orthop. Sci.* 9(1):37–43, 2004.
[19]Jerosch, J., and M. Bischof. Proprioceptive capabilities of the ankle in stable and unstable joints. *Sports Exerc. Inj.* 2:167–171, 1996.
[20]Karlsson, J., and O. Lansinger. Chronic lateral instability of the ankle in athletes. *Sports Med.* 16(5):355–365, 1993.
[21]Lofvenberg, R., J. Karrholm, and B. Lund. The outcome of nonoperated patients with chronic lateral instability of the ankle: a 20-year follow-up study. *Foot Ankle Int.* 15(4):165–169, 1994.
[22]Maffulli, N., and N. A. Ferran. Management of acute and chronic ankle instability. *J. Am. Acad. Orthop. Surg.* 16(10):608–615, 2008.
[23]Messina, D. F., W. C. Farney, and J. C. DeLee. The incidence of injury in Texas high school basketball. A prospective study among male and female athletes. *Am. J. Sports Med.* 27(3):294–299, 1999.
[24]Omori, G., K. Kawakami, M. Sakamoto, T. Hara, and Y. Koga. The effect of an ankle brace on the 3-dimensional kinematics and tibio-talar contact condition for lateral ankle sprains. *Knee Surg. Sports Traumatol. Arthrosc.* 12(5):457–462, 2004.
[25]Perry, J. Gait analysis: normal and pathology function (1st ed.). Thorofare, NJ: Slack Inc., pp. 51–88, 1992.
[26]Povacz, P., S. F. Unger, W. K. Miller, R. Tockner, and H. Resch. A randomized, prospective study of operative and non-operative treatment of injuries of the fibular collateral ligaments of the ankle. *J. Bone Joint Surg. Am.* 80(3):345–351, 1998.
[27]Sharkey, N. A., and A. J. Hamel. A dynamic cadaver model of the stance phase of gait: performance characteristics and kinetic validation. *Clin. Biomech.* 13(6):420–433, 1998.
[28]Siegler, S., J. Block, and C. D. Schneck. The mechanical characteristics of the collateral ligaments of the human ankle joint. *Foot Ankle.* 8(5):234–242, 1988.
[29]Stormont, D. M., B. F. Morrey, K. N. An, and J. R. Cass. Stability of the loaded ankle: relation between articular restraint and primary and secondary static restraints. *Am. J. Sports Med.* 13(5):295–300, 1985.
[30]Taga, I., K. Shino, M. Inoue, K. Nakata, and A. Maeda. Articular cartilage lesions in ankles with lateral ligament injury: an arthroscopic study. *Am. J. Sports Med.* 21(1):120–127, 1993.
[31]Valderrabano, V., M. Horisberger, I. Russell, H. Dougall, and B. Hintermann. Etiology of ankle osteoarthritis. *Clin. Orthop. Relat. Res.* 467(7):1800–1806, 2009.
[32]Valderrabano, V., B. Hintermann, M. Horisberger, and T. S. Fung. Ligamentous posttraumatic ankle osteoarthritis. *Am. J. Sports Med.* 34(4):612–620, 2006.
[33]Verhagen, R. A., G. de Keizer, and C. N. van Dijk. Long-term follow-up of inversion trauma of the ankle. *Arch. Orthop. Trauma Surg.* 114(2):92–96, 1995.
[34]Wan, L., R. J. de Asla, H. E. Rubash, and G. Li. In vivo cartilage contact deformation of human ankle joints under full body weight. *J. Orthop. Res.* 26(8):1081–1089, 2008.
[35]Wickiewicz, T. L., R. R. Roy, P. L. Powell, and V. R. Edgerton. Muscle architecture of the human lower limb. *Clin. Orthop. Relat. Res.* 179:275–283, 1983.
[36]Wright, D. G., and D. C. Rennels. A study of the elastic properties of plantar fascia. *J. Bone Joint Surg. Am.* 46:482–492, 1964.
[37]Zhang, M., and A. F. Mak. In vivo friction properties of human skin. *Prosthet. Orthot. Int.* 23(2):135–141, 1999.